optica

Toward all-fiber supercontinuum spanning the mid-infrared

Darren D. Hudson,[1,*] Sergei Antipov,[1] Lizhu Li,[2] Imtiaz Alamgir,[2] Tomonori Hu,[3] Mohammed El Amraoui,[4] Younes Messaddeq,[4] Martin Rochette,[2] Stuart D. Jackson,[5] and Alexander Fuerbach[1]

[1]Centre for Ultrahigh Bandwidth Devices for Optical Systems (CUDOS), MQ Photonics Research Centre, Department of Physics & Astronomy, Macquarie University, NSW 2109, Australia
[2]Department of Electrical and Computer Engineering, 3480 University Street, McGill University, Montréal H3A 2A7, Canada
[3]Miriad Technologies, 36 Bradfield Road, Lindfield, NSW 2070, Australia
[4]Centre d'Optique, Photonique et Laser, Université Laval, 2375 Rue la Terrasse, Local 2131, Québec G1 V 0A6, Canada
[5]MQ Photonics Research Centre, Department of Engineering, Macquarie University, North Ryde, NSW 2109, Australia
*Corresponding author: darren.hudson@mq.edu.au

Received 15 June 2017; revised 25 August 2017; accepted 25 August 2017 (Doc. ID 298029); published 27 September 2017

Broadband laser light sources in the mid-infrared region attract enormous interest due to the plethora of applications they are enabling, including multispecies trace gas detection, free-space communications, and infrared countermeasures. Key to the progress in supercontinuum generation has been the wide availability of fiber-based near-infrared and bulk-optic mid-infrared pump sources and suitably engineered nonlinear media capable of supporting high-brightness supercontinua. A large proportion of the system complexity relates to the pump source itself with free-space systems based on parametric conversion being the most common for the generation of long-wavelength supercontinua. In an effort to realize all fiber and all mid-infrared supercontinuum sources, we combine a recently developed 2.9 μm ultrafast fiber laser based on holmium with an environmentally stable, polymer-protected all-chalcogenide tapered fiber. By launching 230 fs, 4.2 kW peak power pulses into the As_2Se_3/As_2S_3 tapered fiber, we demonstrate a spectrum spanning from 1.8 to 9.5 μm at the −20 dB points with an average power of more than 30 mW. This >2 octave-spanning supercontinuum is a crucial step toward robust mid-infrared broadband sources required for future field-deployable instruments.

OCIS codes: (190.4370) Nonlinear optics, fibers; (060.2390) Fiber optics, infrared; (190.7110) Ultrafast nonlinear optics; (140.4050) Mode-locked lasers.

https://doi.org/10.1364/OPTICA.4.001163

Supercontinuum sources emitting in the mid-infrared (2–20 μm) have reached a high level of performance, with demonstrations of systems with wide bandwidth and high-power spectral density [1–4], low threshold power [5,6], and in photonic chip integrated planar waveguides [7,8]. The significant research efforts in this space can be largely attributed to practical applications requiring high-brightness mid-IR supercontinua, including trace gas detection [9], remote sensing [10], breath analysis [11], hyperspectral microscopy [12], early-cancer diagnosis [13], and mid-IR frequency combs [14].

Most of the supercontinuum systems demonstrated so far have employed free-space laser systems based on nonlinear optics to produce ultrashort pulses in the mid-IR, which are subsequently coupled to a highly nonlinear waveguide. The nonlinear media used for supercontinuum generation have been extensively explored with devices ranging from step-index fibers [1–3,15], integrated waveguides in both silicon [7] and chalcogenide [8], as well as suspended-core [16] and tapered fibers [4,17–20]. Of these, chalcogenide tapered fibers are particularly appealing as they offer high waveguide nonlinearity and engineerable chromatic dispersion while providing low insertion and propagation losses. These properties enable not only the generation of supercontinua but also a wide range of nonlinear processes, such as optical amplification and laser oscillation based on parametric [21–23] and Raman gains [24].

However, for these systems to be deployable in harsh environments, it is necessary to achieve robust, alignment-free sources of broadband supercontinua with high-power spectral densities. To meet these demanding specifications, much effort has been put into developing all-fiber supercontinuum-based systems. The combination of near-infrared fiber lasers, usually based on thulium at 2 μm, with mid-IR optical fibers has been particularly successful in this approach [25–27]. Indeed, there are currently at least six commercial suppliers (NKT Photonics, Novae, Le Verre Fluore, Leukos, IR Flex, and Thorlabs) of supercontinuum sources with high-brightness spectra extending from 2 to 4 μm. Alternatively, cascading approaches have been demonstrated where a near-IR diode-laser-based supercontinuum is used to pump a mid-IR compatible fiber to further extend the spectral coverage [28]. A logical next step to this all-fiber approach is to extend the wavelength of the ultrafast fiber laser pump to

the mid-IR region and thus extend the supercontinuum bandwidth to much longer wavelengths.

In the current work, we combine a 3 μm class mode-locked fiber laser with a dispersion-engineered As_2Se_3/As_2S_3 fiber taper device to create the widest supercontinuum ever generated in a microwire. The supercontinuum spans over a bandwidth of 10,000 nm (125 THz) in the mid-IR with over 30 mW of average power with no signs of degradation or reduced performance at long operation times. Furthermore, modeling suggests that the long-wavelength edge of the supercontinuum is limited mostly by reduced mode confinement.

The first 3 μm ultrafast fiber lasers were demonstrated in 2015, using the $^4I_{11/2} - {}^4I_{13/2}$ transition in an erbium-doped ZBLAN fiber [29–33]. However, the emission spectrum from these lasers lies directly in a water vapor absorption peak, which limits both the mode-locking performance and the free-space propagation distance. Recently, we reported an ultrafast fiber laser system that employs the holmium ion in fluoride fiber and emits at 2.9 μm, just beyond the atmospheric water vapor absorption [33]. In addition to the propagation improvements, the mode-locking performance was aided by the removal of the intracavity absorption resonances and achieved 37 kW peak power directly from the oscillator.

The current demonstration exploits this system as a pump source and consists of 4 m of Ho^{3+}, Pr^{3+}-codoped ZBLAN fiber and a 1.5 m free-space section containing polarization optics and an isolator (see Fig. 1). We used a new fiber in the experiment that had a core diameter of 12 μm, an NA of 0.12, and was doped with 35,000 ppm Ho^{3+} and 2500 ppm Pr^{3+}. The addition of Pr^{3+} significantly reduces the lower laser level population of Ho^{3+} and efficient lasing on the $^5I_6 - {}^5I_7$ transition at 2.9 μm results. The laser emitted a stable pulse train at a repetition rate of 42 MHz with an average power of 140 mW.

The laser pulses were characterized using a commercial interferometric autocorrelator, revealing a pulse width of 230 fs [see Fig. 2(a)]. The pulse energy was 3.3 nJ, corresponding to a peak power of 12.8 kW at the laser's output. The spectrum [Fig. 2(b)], which was measured using a Yokogawa AQ6376 optical spectrum analyzer (OSA) in high-dynamic-range mode, exhibited a root-mean-square (rms) bandwidth of 47 nm at a central wavelength of 2874 nm. The high-dynamic-range measurement demonstrates that the pulse has spectral content ranging from 2750 to 3000 nm. The time–bandwidth product (TBP) of this laser is 0.39, indicating nearly transform-limited pulse generation, as expected in soliton laser systems. The current cavity length and fiber are different from our previous system [33] but the TBP's are identical. The increased Ho^{3+} doping level relative to the previous system (35,000 ppm versus 30,000 ppm) may be causing lower rates of energy transfer to the Pr^{3+} ion, resulting in some population building up in the lower laser level and hence creating a slightly narrower spectrum (47 nm versus 60 nm).

Figure 3 shows a schematic of the chalcogenide tapered fiber device used to generate the supercontinuum. Light propagating in the device is continuously confined within an As_2Se_3 core surrounded by an As_2S_3 cladding. The device is subdivided into a microwire section (5 cm), in which nonlinear processes take place; transition sections (1.6 cm each), where the profile of the propagating mode is converted adiabatically; and hybrid fiber sections (2.0 cm each side), designed to facilitate coupling from either an input ZBLAN fiber or appropriate free-space coupling optics. The large-core, high-NA hybrid fiber and the low-loss adiabatic taper sections allow us to simultaneously achieve high device throughput and nonlinearity. This is a key benefit of tapered fiber devices that has also recently been exploited using large-mode area chalcogenide photonic crystal fibers [4]. The tapered fiber device is protected with a poly-methyl-methacrylate

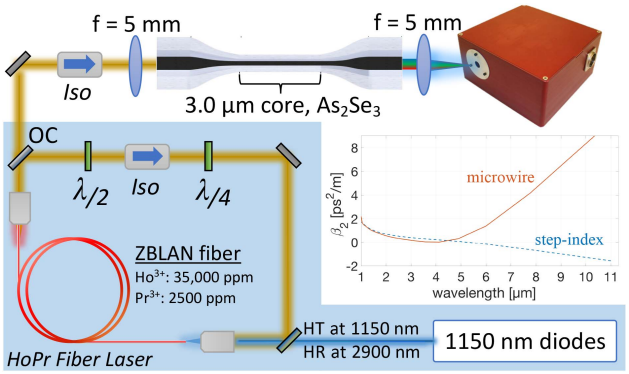

Fig. 1. Layout of the laser cavity and the subsequent supercontinuum generation stage. The holmium laser output passes through an isolator (>40 dB suppression) and is focused into the core of the tapered fiber device using an $f = 5$ mm ZnSe objective lens. The output is collected using an identical lens and focused into a Miriad S3 spectrometer (Miriad Technologies) [36]. The inset shows the dispersion of both the untapered step-index fiber and the microwire section, which was calculated by solving the characteristic equation of an infinite cladding cylindrical waveguide to obtain the propagation constant β.

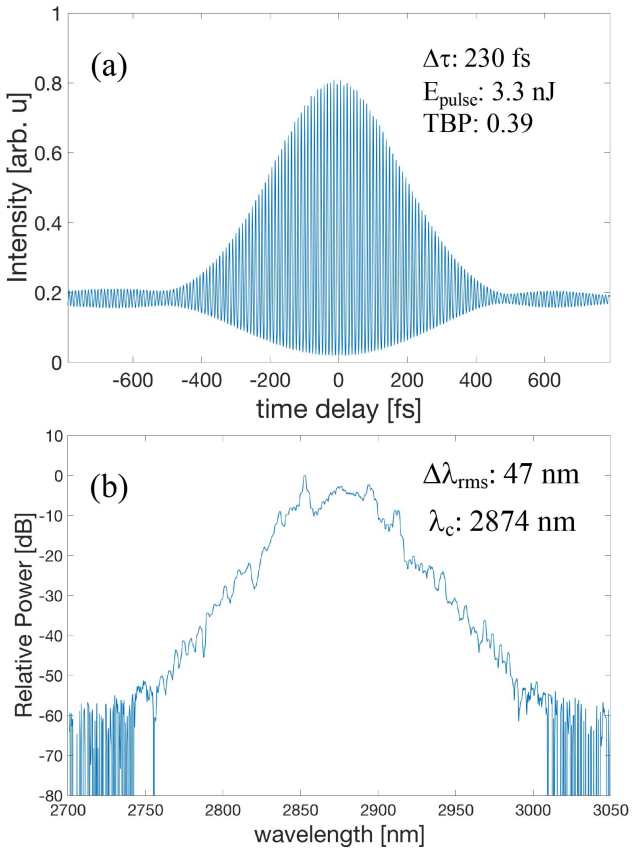

Fig. 2. (a) Autocorrelation and (b) spectrum of the mode-locked laser. The pulse spectrum is centered at 2874 nm with an rms bandwidth of 47 nm. At 50 dB below the peak, the spectrum covers >250 nm.

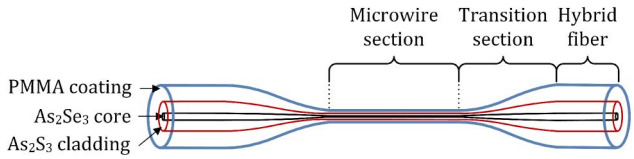

Fig. 3. Tapered fiber device. Pulses are coupled into the hybrid fiber section, where the As_2Se_3 core diameter is 14 μm. The transition sections are 1.6 cm long and the microwire region is 5 cm long with a core diameter of 3.0 μm.

(PMMA) coating, which dramatically increases its overall robustness [34]. The core diameter is 3.0 μm in the microwire and 14.0 μm in the hybrid fiber, while the cladding diameter of the hybrid fiber is 130 μm. The microwire diameter has been optimized to minimize chromatic dispersion at 2.87 μm ($\beta_2 = 0.29$ ps^2/m), leading to normal dispersion at and around the laser emission wavelength. The supercontinuum in all-normal dispersion fibers is driven mainly by two sets of processes: coherent self-phase modulation and optical wave-breaking and incoherent stimulated Raman scattering and four-wave mixing [35]. The nonlinear waveguide parameter of the microwire region is $\gamma = 2.92$ W^{-1}m^{-1} at a wavelength of 2.87 μm.

Before launching into the chalcogenide microwire device, the pulses are first passed through an isolator with >40 dB suppression to prevent back reflections from the high index core of the fiber from coupling back into the laser cavity (see Fig. 1). The pulses are then coupled into the 14 μm input core of the As_2Se_3 taper using an antireflection-coated ZnSe lens with a focal length of 5 mm. To avoid coupling to a cladding mode, the output of the tapered fiber device is imaged using an identical ZnSe lens on the output and a 2D microbolometer focal plane array. Accounting for Fresnel reflections and lens transmission losses, the pulses are coupled to the core with an efficiency of >60%. Upon achieving optimal input coupling, the output lens was used to couple light into a Miriad S3 spectrometer [36], capable of measuring spectra from 1 to 5.5 μm (resolution ~2 nm). For measurements beyond 5.5 μm, we modified the Miriad S3 to use a microbolometer detector, capable of measurements up to 14 μm with a resolution of 5 nm.

At a coupled peak power of 1 kW, the output spectrum showed initial broadening of the pulse spectrum (see Fig. 4). As the coupled peak power was further increased to 4.2 kW, an output supercontinuum was generated with bandwidth ranging from 2 to 12 μm. The broad peak around the pump wavelength is believed to be due to the multimode core of the microwire. The core has a V-number of ~5 and thus supports a few higher-order modes. Coupling to these higher-order modes is minimized by appropriate coupling optics and mounting the microwire device in a straight line with minimal bending. However, by imaging the output of the fiber, some level of higher-order mode power could always be detected. The coupling to these higher-order modes results in a power spectrum density peak around the pump wavelength since higher-order modes do not experience as much waveguide nonlinearity and thus spectral broadening as the fundamental mode.

At the highest pump power, 2.4 octaves of bandwidth (at −30 dB points) is achieved with an average power of >30 mW. As the spectrum reaches long wavelengths relative to the pump, the confinement factor, defined as the ratio of power of the

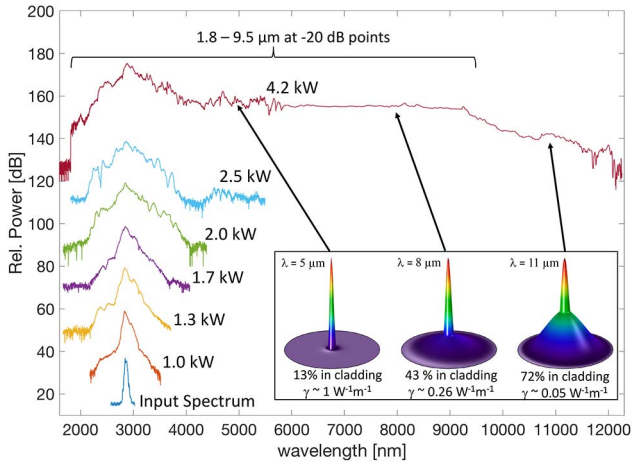

Fig. 4. Spectral expansion at increasing peak power (vertically offset for clarity). The resolution is 2 nm for wavelengths <5.5 μm and 5 nm for longer wavelengths. The inset shows the mode profile in the microwire section (3 μm core diameter) at various wavelengths. The nonlinear parameter γ decreases by a factor of ~20 from 5 to 11 μm.

fundamental mode in the core to the total power of the mode, reduces gradually and thus leads to an increasing fraction of modal power in the As_2S_3 cladding. As shown in the inset of Fig. 4, when the supercontinuum reaches 11 μm, only 28% of the light remains in the core. The reduced nonlinearity due to this core mode expansion leads to a long-wavelength limit of 12 μm.

We numerically investigated the supercontinuum generation by solving the generalized nonlinear Schrödinger equation [37,38]. Our scalar model is based on a frequency-domain formulation that includes the frequency dependence of dispersion, nonlinearity, and effective-mode area. The Raman gain is calculated by considering a delayed Raman response function for As_2Se_3 [39], including an inverse phonon frequency $\tau_1 = 23.2$ fs, a phonon lifetime $\tau_2 = 195$ fs, and a fractional Raman contribution $f_R = 0.10$.

Figure 5 compares the broadest spectrum experimentally obtained with our simulations. Experimentally, the coupled peak power is estimated to be 4.2 kW, while the simulation matches best at a coupled peak power of 3 kW. This discrepancy in peak power can be explained by a loss of the coupled power

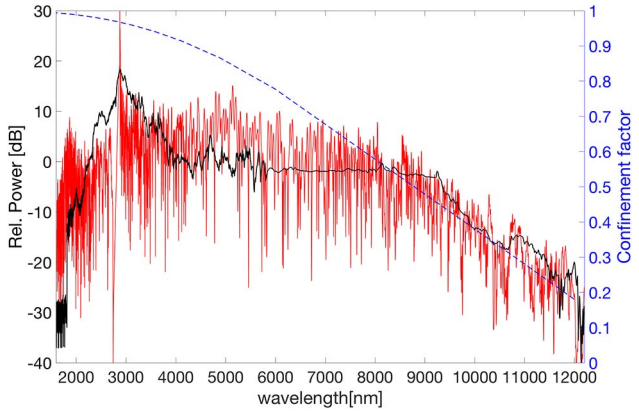

Fig. 5. Broadest supercontinuum generated (black) compared to a nonlinear Schrödinger equation simulation (red). The confinement factor (power in core/total power; blue dashed curve) drops significantly at long wavelengths.

to higher-order modes, as discussed previously. Since the fundamental mode experiences the highest effective nonlinearity due to mode size, the majority of the supercontinuum broadening is due to the power contained within this mode. From the modeling, it appears that we couple around $3.0/4.2 = 71\%$ of the input power into the fundamental mode. Coupling to the fundamental mode could be improved with optimized coupling optics and minimized mode mixing (i.e., an even straighter microwire section). Nevertheless, this coupled peak power combined with the high nonlinear parameter of the microwire leads to a nonlinear phase shift of ~360 rad, and the long-wavelength edge of the supercontinuum reaches 12 μm with −40 dB relative power to the spectral peak. The structured power spectral density features of the simulated spectrum are smoothed out in the experiment due to the limited resolution of the spectrometer, an effect that is more pronounced beyond 5 μm due to the lower dispersion grating used. In addition, pulse-to-pulse variations in the laser will also create a smoothing effect as the measured spectrum is an average of >200,000 spectra.

This level of broadening opens the door for this fiber-based system to be used in applications in the molecular fingerprint region [12] (≈2.5 – 12 μm), including broadband absorption spectroscopy of important trace gasses, such as CO_2, CH_4, and N_2O. As mid-IR fiber components progress, this system will become an all-fiber (i.e., alignment free) source of broadband, coherent light in the 2–12 μm range. Integrated ZBLAN fiber splitters/couplers [40] will allow for fiber ring cavities, and integrated fiber isolators will allow for direct coupling of the laser output to a microwire device.

In summary, we have demonstrated that 3 μm ultrafast fiber laser sources can drive the generation of a supercontinuum that extends across a vast portion of the mid-IR. By launching up to 4.2 kW peak power pulses into a robust polymer-protected As_2Se_3/As_2S_3 fiber taper, we achieve an average power spectral density of $PSD_{average} = 0.003$ mW/nm, spanning 2.4 octaves. While their long-term stability has yet to be characterized, the chalcogenide microwires used in this experiment exhibited no measureable change in transmission over several months of experiments. This result was aided tremendously by the use of a fast spectrometer, which allowed for optimization of the edges of the supercontinuum at frame rates >100 frames per second. Furthermore, significant power exists at various octave points throughout the supercontinuum. Thus, this system represents a good candidate for creating an $f - 2f$ interferometer and ultimately using these lasers as mid-IR frequency comb sources.

Funding. Air Force Office of Scientific Research (AFOSR) (FA2386-16-1-4030); Australian Research Council (ARC) (DP170100531).

REFERENCES

1. T. Cheng, K. Nagasaka, T. Tuan, X. Xue, M. Matsumoto, H. Tezuka, T. Suzuki, and Y. Ohishi, Opt. Lett. **41**, 2117 (2016).
2. Y. Yu, B. Zhang, X. Gai, C. Zhai, S. Qi, W. Guo, Z. Yang, R. Wang, D.-Y. Choi, S. Madden, and B. Luther-Davies, Opt. Lett. **40**, 1081 (2015).
3. R. Gattass, L. B. Shaw, V. Q. Nguyen, P. C. Pureza, I. D. Aggarwal, and J. S. Sanghera, Opt. Fiber Technol. **18**, 345 (2012).
4. C. Petersen, R. Engelsholm, C. Markos, L. Brilland, C. Caillaud, J. Trolès, and O. Bang, Opt. Express **25**, 15336 (2017).
5. X. Li, W. Chen, T. Xue, J. Gao, W. Gao, L. Hu, and M. Liao, Opt. Express **22**, 24179 (2014).
6. A. Al Kadry, M. El Amraoui, Y. Messaddeq, and M. Rochette, Opt. Express **22**, 31131 (2014).
7. N. Singh, D. Hudson, Y. Yu, C. Grillet, S. Jackson, A. Casas-Bedoya, A. Read, P. Atanackovic, S. Duvall, S. Palomba, B. Luther-Davies, S. Madden, D. Moss, and B. Eggleton, Optica **2**, 797 (2015).
8. Y. Yu, X. Gai, P. Ma, D.-Y. Choi, Z. Yang, R. Wang, S. Debbarma, S. Madden, and B. Luther-Davies, Laser Photon. Rev. **8**, 792 (2014).
9. A. Reyes, Z. Hou, E. Mastrigt, R. Horsten, J. Jongste, M. Pijnenburg, H. Urbach, and N. Bhattacharya, Opt. Express **22**, 18299 (2014).
10. S.-L. Girard, M. Allard, M. Piché, and F. Babin, Appl. Opt. **54**, 1647 (2015).
11. R. Bartlome and M. Sigrist, Opt. Lett. **34**, 866 (2009).
12. S. Dupont, C. Petersen, J. Thøgersen, C. Agger, O. Bang, and S. Rud Keiding, Opt. Express **20**, 4887 (2012).
13. A. Seddon, Phys. Status Solidi B **250**, 1020 (2013).
14. A. Schliesser, N. Picqué, and T. Hänsch, Nat. Photonics **6**, 440 (2012).
15. D. Hudson, M. Baudisch, D. Werdehausen, B. Eggleton, and J. Biegert, Opt. Lett. **39**, 5752 (2014).
16. U. Møller, Y. Yu, I. Kubat, C. Petersen, X. Gai, L. Brilland, D. Méchin, C. Caillaud, J. Troles, B.-L. Davies, and O. Bang, Opt. Express **23**, 3282 (2015).
17. A. Marandi, C. Rudy, V. Plotnichenko, E. Dianov, K. Vodopyanov, and R. Byer, Opt. Express **20**, 24218 (2012).
18. C. Baker and M. Rochette, Opt. Express **18**, 12391 (2010).
19. N. Abdukerim and M. Rochette, Opt. Express **24**, 18931 (2016).
20. D. Hudson, E. Mägi, A. Judge, S. Dekker, and B. Eggleton, Opt. Commun. **285**, 4660 (2012).
21. R. Ahmad and M. Rochette, Opt. Express **20**, 9572 (2012).
22. S. Xing, D. Grassani, S. Kharitonov, L. Brilland, C. Caillaud, J. Trolès, and C.-S. Brès, Optica **4**, 643 (2017).
23. R. Ahmad and M. Rochette, Opt. Express **20**, 10095 (2012).
24. N. Abdukerim, L. Li, M. El Amraoui, Y. Messaddeq, and M. Rochette, Appl. Phys. Lett. **110**, 161103 (2017).
25. W. Yang, B. Zhang, K. Yin, X. Zhou, and J. Hou, Opt. Express **21**, 19732 (2013).
26. A. Heidt, J. Price, C. Baskiotis, J. S. Feehan, Z. Li, S. Alam, and D. Richardson, Opt. Express **21**, 24281 (2013).
27. K. Liu, J. Liu, H. Shi, F. Tan, and P. Wang, Opt. Express **22**, 24384 (2014).
28. C. Petersen, P. Moselund, C. Petersen, U. Møller, and O. Bang, Opt. Express **24**, 749 (2016).
29. T. Hu, S. Jackson, and D. Hudson, Opt. Lett. **40**, 4226 (2015).
30. S. Duval, M. Bernier, V. Fortin, J. Genest, M. Piché, and R. Vallée, Optica **2**, 623 (2015).
31. S. Duval, M. Olivier, V. Fortin, M. Bernier, M. Piché, and R. Vallée, Proc. SPIE **9728**, 972802 (2016).
32. D. Hudson, Opt. Fiber Technol. **20**, 631 (2014).
33. S. Antipov, D. Hudson, A. Fuerbach, and S. Jackson, Optica **3**, 1373 (2016).
34. C. Baker and M. Rochette, IEEE Photon. J. **4**, 960 (2012).
35. A. Heidt, J. Feehan, J. Price, and T. Feurer, J. Opt. Soc. Am. B **34**, 764 (2017).
36. https://www.miriad-tech.com.
37. J. Dudley and J. R. Taylor, eds., *Supercontinuum Generation in Optical Fibers* (Cambridge, 2010).
38. J. Lægsgaard, Opt. Express **15**, 16110 (2007).
39. J. Hu, C. Menyuk, L. Shaw, J. Sanghera, and I. Aggarwal, Opt. Express **18**, 6722 (2010).
40. S. Gross, N. Jovanovic, A. Sharp, M. Ireland, J. Lawrence, and M. Withford, Opt. Express **23**, 7946 (2015).